Comparative study of three-nucleon potentials in nuclear matter

Alessandro Lovato,[1,2] Omar Benhar,[2,3] Stefano Fantoni,[4] and Kevin E. Schmidt[5]

[1]*SISSA, IT-34014 Trieste, Italy*
[2]*INFN, Sezione di Roma, IT-00185 Roma, Italy*
[3]*Dipartimento di Fisica, Università "La Sapienza," IT-00185 Roma, Italy*
[4]*ANVUR, National Agency for the Evaluation of Universities and Research Institutes, Piazzale Kennedy, 20, IT-00144 Roma, Italy*
[5]*Department of Physics, Arizona State University, Tempe, Arizona 85287, USA*

A new generation of local three-body potentials providing an excellent description of the properties of light nuclei, as well as of the neutron-deuteron doublet scattering length, has been recently derived. We have performed a comparative analysis of the equations of state of both pure neutron matter (PNM) and symmetric nuclear matter (SNM) at zero temperature obtained using these models of three-nucleon forces. In particular, we have carried out both variational and auxiliary field diffusion Monte Carlo calculations of the equation of state of PNM, while in the case of SNM we have only the variational approach has been considered. None of the considered potentials simultaneously explains the empirical equilibrium density and binding energy of symmetric nuclear matter. However, two of them provide reasonable values of the saturation density. The ambiguity concerning the treatment of the contact term of the chiral inspired potentials is discussed.

I. INTRODUCTION

The definition of the potential describing three-nucleon interactions is a central issue of nuclear many-body theory. Three-nucleon forces (TNFs) have long been known to provide a sizable contribution to the energies of the ground and low-lying excited states of light nuclei and play a critical role in determining the equilibrium properties of symmetric nuclear matter. In addition, their effect is expected to become large, or even dominant, in high-density neutron matter, the understanding of which is required for the theoretical description of compact stars.

Ab initio nuclear many-body approaches are based on the premise that the dynamics can be modeled studying exactly solvable systems, having mass number $A \leqslant 3$. This is a most important feature because, owing to the complexity of strong interactions and the prohibitive difficulties associated with the solution of the quantum mechanical many-body problem, theoretical calculations of nuclear observables generally involve a number of approximations. Hence, models of nuclear dynamics extracted from analyses of the properties of complex nuclei are plagued by the systematic uncertainty associated with the use of a specific approximation scheme.

Highly realistic two-nucleon potentials, either purely phenomenological [1–4] or based on chiral perturbation theory (ChPT) [5,6], have been obtained from accurate fits of the properties of the bound and scattering states of the two-nucleon system [7–13]. Unfortunately, however, the extension to the case of the three-nucleon potential is not straightforward. Phenomenological models, such as the Urbana IX (UIX) potential, that reproduce the observed binding energy of ^{3}H by construction, fail to explain the measured nd doublet scattering length, $^2a_{nd}$ [14], as well as the proton analyzing power in p-^{3}He scattering, A_y [15].

In recent years, the scheme based on ChPT has been extensively employed to obtain three-nucleon potential models [16,17]. The main advantage of this approach is the possibility of treating the nucleon-nucleon (*NN*) potential and the TNFs in a more consistent fashion, as the parameters c_1, c_3, and c_4, fixed by *NN* and πN data, are also used in the definition of the TNFs. In fact, the next-to-next-to-leading-order (NNLO) three-nucleon interaction only involves two parameters, namely, c_D and c_E, that do not appear in the *NN* potential and have to be determined fitting low-energy three-nucleon (*NNN*) observables. Unfortunately, however, πN and *NN* data still leave some uncertainties on the c_i's, that cannot be completely determined by *NNN* observables.

A comprehensive comparison between purely phenomenological and *chiral inspired* TNFs, which must necessarily involve the analysis of both pure neutron matter and symmetric nuclear matter, is made difficult by the fact that chiral TNFs are derived in momentum space, while many theoretical formalisms are based on the coordinate space representation.

The local, coordinate space, form of the chiral NNLO three-nucleon potential, hereafter referred to as NNLOL, can be found in Ref. [18]. However, establishing a connection between momentum and coordinate space representations involves some subtleties.

The authors of Ref. [16] have shown that the NNLO (momentum space) three-body potential obtained from the chiral Lagrangian, when operating on a antisymmetric wave function, gives rise to contributions that are not all independent of one another. To obtain a local potential in coordinate space one has to regularize using the momenta transferred among the nucleons. This regularization procedure makes all the terms of the chiral potential independent, so that, in principle, all of them have to be taken into account. The potential would otherwise be somewhat inconsistent, as it becomes apparent in nuclear matter calculations, which involve larger momenta.

A comparative study of different three-nucleon local interactions [Urbana UIX (UIX), chiral inspired revision of

Tucson-Melbourne (TM$'$), and chiral NNLOL three-body potential], used in conjunction with the local Argonne v_{18} *NN* potential, has been recently performed [19]. The authors of Ref. [19] used the hyperspherical harmonics formalism to compute the binding energies of ^{3}H and ^{4}He, as well as the *nd* doublet scattering length, and found that the three-body potentials do not simultaneously reproduce these quantities. Selecting different sets of parameters for each TNF they were able to obtain results compatible with experimental data, although a unique parametrization for each potential has not been found. This problem is a consequence of the fact that the three low-energy observables considered are not enough to completely fix the set of parameters entering the definition of the potentials.

The work described in this paper is aimed at testing the different parametrization of the potentials in nuclear matter. In the case of symmetric nuclear matter (SNM), a *realistic* equation of state (EoS) is constrained by the available empirical information on saturation density, ρ_0, binding energy per nucleon at equilibrium, E_0, and compressibility, K. Furthermore, the recent observation of a neutron star of about two solar masses [20] puts a constraint on the stiffness of the EoS of β-stable matter, closely related to that of PNM.

Nuclear matter calculations are carried out using a variety of many-body approaches. The scheme referred to as FHNC/SOC, based on correlated basis functions and the cluster expansion technique, has been first used to perform accurate nuclear-matter calculations with realistic three-body potentials in Ref. [21]. This analysis included early versions of both the Urbana (UIV, UV) and the Tucson-Melbourne (TM) three-body interactions with the set of parameters reported in Ref. [22]. The results indicate that the UV model, the only one featuring a phenomenological repulsive term, provides a reasonable nuclear-matter saturation density, while the UIV and TM potentials fail to predict saturation. In addition, none of the considered models yields reasonable values of the SNM binding energy and compressibility.

The findings of Ref. [21] are similar to those obtained in Ref. [23], whose authors took into account additional diagrams of the cluster expansion and used the UVII model. The state-of-the-art variational calculations discussed in Ref. [24], carried out using the Argonne v_{18} [3] and UIX [25] potentials, also sizably underbinds SNM. While the authors of Ref. [24] ascribed this discrepancy to deficiencies of the variational wave function, the analysis of Refs. [26,27] suggests that this problem can be largely attributable to the uncertainties associated with the description of three-nucleon interactions, whose contribution turns out to be significant.

Momentum space chiral three-body interaction have been also employed in nuclear matter [28–30]. In these studies, the NNNLO chiral two-body potential has been evolved to low-momentum interaction $V_{\text{low}\,k}$, suitable for standard perturbation theory in the Fermi gas basis. The results, showing that the TNF is essential to obtain saturation and realistic equilibrium properties of SNM [28,29], exhibit a sizable cutoff dependence. At densities around the saturation point this effect is $\sim$4 MeV. In addition, different values of the constants c_i lead to different equations of state for SNM [29] and pure neutron matter (PNM) [30].
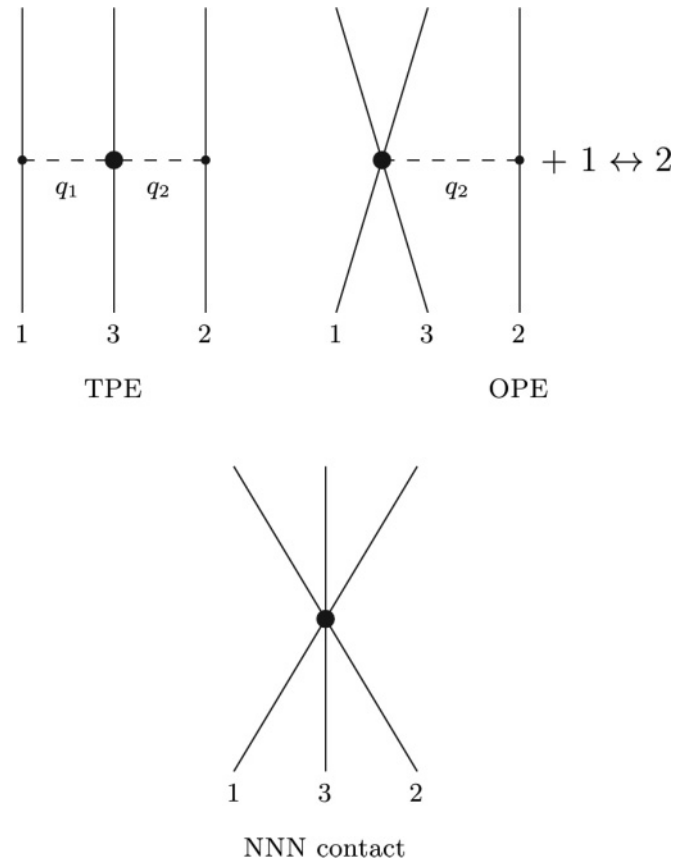

FIG. 1. TPE, OPE, and *NNN* contact interactions of the chiral three-body force at NNLO.

The main features of the chiral inspired TNFs are briefly reviewed in Sec. II, while in Sec. III we analyze the coordinate space form of the TNFs derived in Ref. [19], and discuss several issues related to the calculation of their contributions in nuclear matter. We have carried out both FHNC/SOC and auxiliary field diffusion Monte Carlo (AFDMC) calculations of the EoS of cold PNM, while in the case of SNM only the variational approach has been used. The numerical results of these calculations are discussed in Sec. IV. Finally, in Sec. V we summarize our findings and state the conclusions.

II. CHIRAL INSPIRED MODELS OF THREE NUCLEON FORCES

In a chiral theory without Δ degrees of freedom, the first nonvanishing three-nuclon interactions appear at NNLO in the Weinberg power counting scheme [31,32]. The interaction is described by three different physical mechanisms, corresponding to three different topologies of Feynman diagrams, drawn in Fig. 1 [16]. The first two diagrams correspond to two-pion exchange (TPE) and one-pion exchange (OPE) with the pion emitted (or absorbed) by a contact *NN* interaction. The third diagram represents a contact three-nucleon interaction.

The full expression for the TNFs is obtained by summing all possible permutations of the three nucleons. For this kind of potential, it turns out that there are only three independent
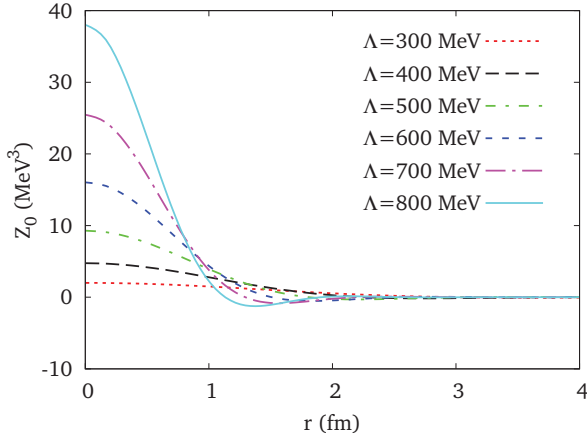
FIG. 2. (Color online) Radial dependence of the function $Z_0(r)$, appearing in Eq. (27), plotted for different values of the cutoff Λ.

cyclic permutations, that is,

$$V^\chi(1, 23) = V^\chi(1 : 23) + V^\chi(2 : 13) + V^\chi(3 : 12). \quad (1)$$

The Feynman diagrams of Fig. 1 refer to the permutation $(3 : 12)$, which can be written as

$$V^\chi(3 : 12) = c_1 V_1(3 : 12) + c_3 V_3(3 : 12) + c_4 V_4(3 : 12)$$
$$+ c_D V_D(3 : 12) + c_E V_E(3 : 12). \quad (2)$$

The first three terms V_1, V_3, and V_4 come from the TPE diagram and are related to πN scattering. In particular, V_1 describes the S-wave contribution, while V_3 and V_4 are associated with the P wave. The other terms, V_D and V_E, are the OPE and contact contributions, respectively. Their momentum space expressions are [16]

$$\tilde{V}_1(3 : 12) = -V_0 m_\pi^2 \, \tau_{12} \frac{(\boldsymbol{\sigma}_1 \cdot \mathbf{q}_1)}{(q_1^2 + m_\pi^2)} \frac{(\boldsymbol{\sigma}_2 \cdot \mathbf{q}_2)}{(q_2^2 + m_\pi^2)},$$

$$\tilde{V}_3(3 : 12) = \frac{V_0}{2} \, \tau_{12} \frac{(\boldsymbol{\sigma}_1 \cdot \mathbf{q}_1)}{(q_1^2 + m_\pi^2)} \frac{(\boldsymbol{\sigma}_2 \cdot \mathbf{q}_2)}{(q_2^2 + m_\pi^2)} \mathbf{q}_1 \cdot \mathbf{q}_2,$$

$$\tilde{V}_4(3 : 12) = \frac{V_0}{4} \, \boldsymbol{\tau}_3 \cdot (\boldsymbol{\tau}_1 \times \boldsymbol{\tau}_2) \frac{(\boldsymbol{\sigma}_1 \cdot \mathbf{q}_1)}{(q_1^2 + m_\pi^2)} \frac{(\boldsymbol{\sigma}_2 \cdot \mathbf{q}_2)}{(q_2^2 + m_\pi^2)}$$
$$\boldsymbol{\sigma}_3 \cdot (\mathbf{q}_1 \times \mathbf{q}_2), \quad (3)$$

$$\tilde{V}_D(3 : 12) = -V_0^D \tau_{12} \left[\frac{(\boldsymbol{\sigma}_2 \cdot \mathbf{q}_2)}{(q_2^2 + m_\pi^2)} (\boldsymbol{\sigma}_1 \cdot \mathbf{q}_2) \right.$$
$$\left. + \frac{(\boldsymbol{\sigma}_1 \cdot \mathbf{q}_1)}{(q_1^2 + m_\pi^2)} (\boldsymbol{\sigma}_2 \cdot \mathbf{q}_1) \right],$$

$$\tilde{V}_E(3 : 12) = V_0^E \tau_{12}.$$

where $\boldsymbol{\sigma}_i$ and $\boldsymbol{\tau}_i$ are the Pauli matrices describing the spin and the isospin of particle i. With σ_{ij} and τ_{ij} we denote the scalar product $\boldsymbol{\sigma}_i \cdot \boldsymbol{\sigma}_j$ and $\boldsymbol{\tau}_i \cdot \boldsymbol{\tau}_j$, respectively. The strengths of the TPE, OPE, and contact terms V_0, V_0^D, and V_0^E are given by

$$V_0 = \left(\frac{g_A}{F_\pi^2} \right)^2, \quad V_0^D = \frac{g_A}{8 F_\pi^4 \Lambda_\chi}, \quad V_0^E = \frac{1}{F_\pi^4 \Lambda_\chi}, \quad (4)$$

where $g_A = 1.29$ is the axial-vector coupling constant, $F_\pi = 92.4$ MeV is the weak pion decay constant and Λ_χ is the chiral symmetry-breaking scale, of the order of the ρ meson mass.

The low-energy constants (LECs) c_1, c_3, and c_4 also appear in the subleading TPE term of the chiral NN potential and are fixed by πN [33,34] and/or NN [5] data. The parameters c_D and c_E are specific to the three-nucleon interaction and have to be fixed using NNN low-energy observables, such as the ^{3}H binding energy and the nd doublet scattering length $^2 a_{nd}$ [16].

The many-body methods employed in our work, namely, FHNC/SOC and AFDMC, require a local expression of the three-body potential in coordinate space, that can be obtained performing the Fourier transform [18]

$$V^\chi(3 : 12) = \int \frac{d^3 q_1}{(2\pi)^3} \frac{d^3 q_2}{(2\pi)^3} \tilde{V}^\chi(3 : 12)$$
$$\times F_\Lambda(q_1^2) F_\Lambda(q_2^2) e^{i \mathbf{q}_1 \cdot \mathbf{r}_{13}} e^{i \mathbf{q}_2 \cdot \mathbf{r}_{23}}, \quad (5)$$

where the cutoff functions F_Λ, defined as

$$F_\Lambda(q_i^2) = \exp\left(-\frac{q_i^4}{\Lambda^4} \right), \quad (6)$$

can depend on the momenta transferred among the nucleons, q_i, only. This feature has important consequences for the OPE and contact terms, which will be discussed at a later stage.

The cutoff Λ in the previous equation, while not being required to be the same as Λ_χ, is of the same order of magnitude. Choosing the fourth power of the momentum in Eq. (6) is therefore convenient, as the regulator generates powers of q/Λ that are beyond NNLO in the chiral expansion.

The Fourier transform can be readily computed and provides the following coordinate-space representation of the chiral three-body potential:

$$V_1(3 : 12) = W_0 \tau_{12} (\boldsymbol{\sigma}_1 \cdot \vec{r}_{13})(\boldsymbol{\sigma}_2 \cdot \vec{r}_{23}) y(r_{13}) y(r_{23}),$$

$$V_3(3 : 12) = W_0 \tau_{12} [\sigma_{12} y(r_{13}) y(r_{23})$$
$$+ (\boldsymbol{\sigma}_1 \cdot \vec{r}_{23})(\boldsymbol{\sigma}_2 \cdot \vec{r}_{23}) t(r_{23}) y(r_{13})$$
$$+ (\boldsymbol{\sigma}_1 \cdot \vec{r}_{13})(\boldsymbol{\sigma}_2 \cdot \vec{r}_{13}) t(r_{13}) y(r_{23})$$
$$+ (\vec{r}_{13} \cdot \vec{r}_{23})(\boldsymbol{\sigma}_1 \cdot \vec{r}_{13})(\boldsymbol{\sigma}_2 \cdot \vec{r}_{23}) t(r_{13}) t(r_{23})],$$

$$V_4(3 : 12) = W_0 (\boldsymbol{\tau}_3 \cdot \boldsymbol{\tau}_1 \times \boldsymbol{\tau}_2)[(\boldsymbol{\sigma}_3 \cdot \boldsymbol{\sigma}_2 \times \boldsymbol{\sigma}_1) y(r_{13}) y(r_{23})$$
$$+ (\boldsymbol{\sigma}_3 \cdot \vec{r}_{23} \times \boldsymbol{\sigma}_1)(\boldsymbol{\sigma}_2 \cdot \vec{r}_{23}) t(r_{23}) y(r_{13})$$
$$+ (\boldsymbol{\sigma}_2 \cdot \vec{r}_{13} \times \boldsymbol{\sigma}_3)(\boldsymbol{\sigma}_1 \cdot \vec{r}_{13}) t(r_{13}) y(r_{23})$$
$$+ (\boldsymbol{\sigma}_3 \cdot \vec{r}_{23} \times \vec{r}_{13})(\boldsymbol{\sigma}_1 \cdot \vec{r}_{13})(\boldsymbol{\sigma}_2 \cdot \vec{r}_{23}) t(r_{13}) t(r_{23})],$$

$$V_D(3 : 12) = W_0^D \tau_{12} [\sigma_{12} y(r_{23}) z_0(r_{13})$$
$$+ (\boldsymbol{\sigma}_1 \cdot \vec{r}_{23})(\boldsymbol{\sigma}_2 \cdot \vec{r}_{23}) t(r_{23}) z_0(r_{13})$$
$$+ \sigma_{12} y(r_{13}) z_0(r_{23})$$
$$+ (\boldsymbol{\sigma}_2 \cdot \vec{r}_{13})(\boldsymbol{\sigma}_1 \cdot \vec{r}_{13}) t(r_{13}) z_0(r_{23})],$$

$$V_E(3 : 12) = W_0^E \tau_{12} z_0(r_{13}) z_0(r_{23}), \quad (7)$$

where W_0, W_0^D and W_0^E are obtained multiplying the corresponding V_0, V_0^D, and V_0^E by a factor $m_\pi^6/(4\pi)^2$. The radial

functions appearing in the above equations are defined as

$$y(r) = \frac{z_1'(r)}{r},$$

$$t(r) = \frac{1}{r^2}\left[z_1''(r) - \frac{z_1'(r)}{r}\right] = \frac{1}{r}y'(r), \quad (8)$$

while z_n, proportional to Z_n introduced in Ref. [22], is given by

$$z_n(r) = \frac{4\pi}{m_\pi^3} \int \frac{d^3q}{(2\pi)^3} \frac{F_\Lambda(q^2)}{(q^2 + m_\pi^2)^n} e^{i\mathbf{q}\cdot\mathbf{r}}$$

$$= \frac{2}{\pi m_\pi^3} \int dq\, q^2 \frac{F_\Lambda(q^2)}{(q^2 + m_\pi^2)^n} j_0(qr), \quad (9)$$

with $j_0(x) = \sin(x)/x$. Note that, owing to the form of the cutoff function of Eq. (6), the radial functions are not known in analytic form and must be obtained from a numerical integration.

Recently, the authors of Ref. [19] have studied the low-energy *NNN* observables using the hyperspherical harmonics formalism and a nuclear Hamiltonian including the NNLOL potential and the Argonne v_{18} [3] two-body interaction.

This mixed approach requires a fit of all the LECs appearing in the chiral three-body interaction, not c_D and c_E only. Hence consistency in the treatment of two- and three- nucleon interactions, which would be achievable using a Hamiltonian in which all potentials are derived from chiral effective theory, is lost. Nevertheless, it is possible to exploit ChPT to assess the importance of the different terms contributing to the TNFs. This procedure allows one to select the most relevant spin-isospin structures entering the three-nucleon potential, as well as the shape of the corresponding radial functions.

Within the chiral approach, to obtain a potential yielding a fit to the experimental data of accuracy comparable to that achieved by the Argonne v_{18} model, one has to include terms up to NNNLO [9,10]. As a consequence, a fully consistent calculation, in principle, requires a NNNLO three-body interaction, the expression of which has been only recently derived in Ref. [35]. It turns out that some of the terms appearing at NNNLO can be taken into account shifting the constants c_i of about 20%–30% with respect to their original values [17]. This procedure has been followed in precision studies of TNFs. By fitting all the LECs of the NNLOL interaction, the authors of Ref. [19] have improved upon the NNLO approximation, as they have effectively included the corrections to the c_i appearing at NNNLO level.

The best-fit parameters for the ^{3}H and ^{4}He binding energies and for the *nd* scattering length, $^2a_{nd}$, are listed in Table I. For all the different parametrizations, denoted by NNLOL$_i$, c_1 and

TABLE I. Parameters of the NNLOL interactions of Ref. [19].

Potential	c_3 (MeV^{-1})	c_4 (MeV^{-1})	c_D	c_E
NNLOL$_1$	−0.00448	−0.001963	−0.5	0.100
NNLOL$_2$	−0.00448	−0.002044	−1.0	0.000
NNLOL$_3$	−0.00480	−0.002017	−1.0	−0.030
NNLOL$_4$	−0.00544	−0.004860	−2.0	−0.500

Λ_χ have been fixed to their original values 0.00081 MeV^{-1} and 700 MeV, respectively [16]. The momentum cutoff of Eq. (6) has been set to 500 MeV.

As noticed in Ref. [36], despite the different underlying physical mechanisms, both TM and UIX three-nucleon interactions can be written as a sum of terms of the same form as those appearing in Eq. (7). The differences among NNLOL, TM, and UIX lie in the constants and in the radial functions.

The TM$'$ potential only involves the V_1, V_3, and V_4 contributions [37]. The cutoff function for this potential is not the same as in Eq. (6), but

$$F_\Lambda(q^2) = \left(\frac{\Lambda^2 - m_\pi^2}{\Lambda^2 + q^2}\right)^2. \quad (10)$$

The above form allows for the analytical integration of Eq. (9), yielding the radial functions

$$y(r) = \frac{e^{-r\Lambda}}{2m_\pi^3 r^3}\big[2 - m_\pi^2 r^2 - 2(1 + m_\pi r)e^{r(\Lambda - m_\pi)}$$

$$+ r\Lambda(2 + r\Lambda)\big],$$

$$t(r) = \frac{e^{-r\Lambda}}{2m_\pi^3 r^5}\big\{-6 + 2\big(3 + 3m_\pi r + m_\pi^2 r^2\big)e^{r(\Lambda - m_\pi)}$$

$$+ m_\pi^2 r^2(1 + r\Lambda) - r\Lambda[6 + r\Lambda(3 + r\Lambda)]\big\}. \quad (11)$$

The TM$'$ potential corresponds to the following choice of the strength constants [compare to Eq. (7)]:

$$W_0 = \left(\frac{gm_\pi}{8\pi m_N}\right)^2 m_\pi^4 \quad (12)$$

and

$$c_1 = \frac{a}{m_\pi^2}, \quad c_3 = 2b, \quad c_4 = -4d, \quad (13)$$

a, b, and c being the parameters entering the definition of the TM$'$ potential [37]. The authors of Ref. [19] have determined the parameters of the TM$'$ potential fitting the same set of low-energy *NNN* observables employed for the NNLOL potential. To get a better description of the experimental data, they introduced a repulsive three-nucleon contact term, similar to the chiral V_E, but with τ_{12} omitted,

$$V_E(3:12) = W_0^E z_0(r_{13})z_0(r_{23}), \quad (14)$$

where

$$W_0^E = \left(\frac{gm_\pi}{8\pi m_N}\right)^2 \frac{9m_\pi^2}{\Lambda_\chi}. \quad (15)$$

The corresponding radial function can be computed analytically from Eq. (9):

$$z_0(r) = \frac{e^{-r\Lambda}}{8\pi\Lambda}\big(m_\pi^2 - \Lambda^2\big)^2. \quad (16)$$

As in the original paper [22], in Ref. [19] the value of the pion-nucleon coupling constant is set to $g^2 = 179.7$ MeV, the pion mass is $m_\pi = 139.6$ MeV and the nucleon mass is defined through the ratio $m_N/m_\pi = 6.726$. The symmetry breaking scale Λ_χ of Eq. (15) has the same value, 700 MeV, used for the NNLOL potential.

TABLE II. Parameters of the TM′ potential reproducing the low-energy *NNN* experimental data with $a = -0.87\, m_\pi^{-1}$ [19].

Potential	$b(m_\pi^{-3})$	$d(m_\pi^{-3})$	c_E	$\Lambda(m_\pi)$
TM′$_1$	−8.256	−4.690	1.0	4.0
TM′$_2$	−3.870	−3.375	1.6	4.8
TM′$_3$	−2.064	−2.279	2.0	5.6

The parameters of the TM′ potentials, TM′$_i$, that according to Ref. [19] reproduce the binding energies of ^{3}H and ^{4}He and $^2a_{nd}$, are listed in Table II. It turns out that V_1, gives a very small contribution to the low-energy *NNN* observables. Therefore, the parameter a has been kept to its original value of $-0.87\, m_\pi^{-1}$.

The Fujita Miyazawa term [38] of the UIX potential [25], $V^{2\pi}$, describing the process whereby two pions are exchanged among nucleons and a Δ resonance is excited in the intermediate state, is conveniently written as

$$\hat{V}^{2\pi}(3:12) = A_{2\pi}\{\hat{X}_{13}, \hat{X}_{23}\}\{\tau_{13}, \tau_{23}\} + C_{2\pi}[\hat{X}_{13}, \hat{X}_{23}][\tau_{13}, \tau_{23}], \tag{17}$$

where

$$\hat{X}_{ij} = Y(m_\pi r)\sigma_{ij} + T(m_\pi r)S_{ij}, \tag{18}$$

and

$$S_{ij} = 3(\hat{r}_{ij} \cdot \boldsymbol{\sigma}_i)(\hat{r}_{ij} \cdot \boldsymbol{\sigma}_j) - \sigma_{ij} \tag{19}$$

is the tensor operator. The radial functions associated with the spin and tensor components read

$$Y(x) = \frac{e^{-x}}{x}\xi_Y(x), \tag{20}$$

$$T(x) = \left(1 + \frac{3}{x} + \frac{3}{x^2}\right)Y(x)\xi_T(x), \tag{21}$$

and the $\xi(x)$ are short-range cutoff functions defined as

$$\xi_Y(x) = \xi_T(x) = 1 - e^{-cx^2}. \tag{22}$$

In the original derivation of the UIX potential the ratio $C_{2\pi}/A_{2\pi}$ was fixed to 1/4 and the cutoff parameter was $c = 2.1$ fm^{-2}, the same value as in the cutoff functions of the OPE term of the Argonne v_{18} two-body potential.

It can be shown that the anticommutator and commutator terms correspond to V_3 and V_4 of Eq. (7), provided the relations between the constants

$$\begin{aligned} bW_0 &= 4A_{2\pi}, \\ dW_0 &= 4C_{2\pi} \end{aligned} \tag{23}$$

and the radial functions

$$\begin{aligned} Y(r) &= y(r) + \frac{r^2}{3}t(r), \\ T(r) &= \frac{r^2}{3}t(r) \end{aligned} \tag{24}$$

are satisfied.

The repulsive term of the UIX potential,

$$V^R(3:12) = U_0 T^2(m_\pi r_{13})T^2(m_\pi r_{23}), \tag{25}$$

is equivalent to the V_E term appearing in the TM′ potential and (aside from the τ_{12} factor) in the NNLOL chiral potential if the following relations hold:

$$T^2(m_\pi r) = z_0(r), \quad U_0 = c_E W_0^E. \tag{26}$$

The UIX potential was not designed to reproduce low-energy *NNN* observables only. While the parameter $A_{2\pi}$ was obtained from the fit of the observed binding energy of ^{3}H, the strength U_0, was indeed adjusted to reproduce the empirical saturation density of SNM, $\rho_0 = 0.16$ fm^{-3}.

In Ref. [19] it has been found that the original parametrization of the UIX potential underestimates $^2a_{nd}$ and slightly overbinds ^{4}He.

The authors of Ref. [19] have calculated the differential cross section and the vector and tensor analyzing powers of *p*-*d* scattering at $E_{\text{lab}} = 3$ MeV for the different parametrizations of NNLOL and TM′ potentials. They found that all of them lead to underestimating A_y (the so-called A_y puzzle remains unsolved) and T_{11}, while the central minimum in T_{21} is always overestimated. However, the NNLOL model provides a slight improvement with respect to the UIX potential in the description of the polarization observables. However, no substantial modifications from the UIX results are given by the TM′ interactions.

III. THREE-NUCLEON POTENTIALS IN NUCLEAR MATTER

The investigation of uniform nuclear matter may shed light on both the nature and the parametrization of the TNFs, although the quantitative description of this system cannot be achieved within a mere generalization of the approaches developed for light nuclei. In this section, we analyze the structure of the contact term of the NNLOL potential of Ref. [19] and discuss the calculation of the TNF contribution to nuclear-matter energy.

A. NNLOL contact term issue

While the NNLOL chiral interactions provide a fully consistent description of the binding energies of ^{3}H and ^{4}He, as well as of the scattering length $^2a_{nd}$, some ambiguities emerge when these interactions are used to calculate the nuclear-matter EoS.

For our purposes, it is convenient to rewrite the NNLOL chiral contact term of Eq. (7) in the form

$$V_E^\tau(3:12) = V_0^E \tau_{12} Z_0(r_{13})Z_0(r_{23}), \tag{27}$$

where the superscript τ has a meaning that will be soon clarified. The radial function $Z_0(r) = m_\pi^3/(4\pi)z_0(r)$ approaches the Dirac δ function in the limit of infinite cutoff, as shown in Fig. 2. Strictly speaking, the local version of V_E is a genuine "contact term" in this limit only, while for finite values of the cutoff it acquires a finite range.

In addition to V_E^τ of Eq. (27), the chiral expansion leads to the appearance of five spin-isopin structures in the contact

term. For example, the scalar contribution is

$$V_E^I(3:12) = V_0^E Z_0(r_{13}) Z_0(r_{23}). \tag{28}$$

Within this context, the superscripts τ and I identify the τ_{12} and scalar contact terms, respectively.

In Ref. [16] it has been shown that, once the sum over all cyclic permutation is performed, all contributions to the product between the potential and the antisymmetrization operator $\mathcal{A}_{123}$ have the same spin-isospin structure. Therefore, it is convenient to take into account just one of the contact terms. This result was obtained in momentum space, without the cutoff functions F_Λ. As a consequence, in coordinate space it only holds true in the limit of infinite cutoff. In particular, for $V_E^\tau(3:12)$ and $V_E^I(3:12)$, it turns out that

$$\sum_{\text{cycl}} V_0^E \delta(\mathbf{r}_{13}) \delta(\mathbf{r}_{23}) \tau_{12} \mathcal{A}_{123} = -\sum_{\text{cycl}} V_0^E \delta(\mathbf{r}_{13}) \delta(\mathbf{r}_{23}) \mathcal{A}_{123}, \tag{29}$$

making these two terms equivalent. The limit of infinite cutoff is crucial, because the radial part of the exchange operator, when multiplied by the Dirac δ functions, is nothing but the identity

$$e^{i\mathbf{k}_{ij}\cdot\mathbf{r}_{ij}} \delta(\mathbf{r}_{ij}) = \delta(\mathbf{r}_{ij}). \tag{30}$$

After the regularization, that is, with the δ function replaced with Z_0, the proof is spoiled and the six different structures are no longer equivalent.

In PNM contact terms involving three or more neutrons vanish because of the Pauli principle. However, the expectation value of the contact terms of the NNLOL potential can be different from zero.

Let us assume that reproducing the binding energies of light nuclei and $^2a_{nd}$ require a repulsive V_E. Then one has to choose either $c_E^{\tau_{12}} < 0$ or $c_E^I > 0$. In PNM, as

$$\langle \tau_{12} \rangle_{\text{PNM}} = 1, \tag{31}$$

it turns out that V_E^τ is attractive and V_E^I is repulsive. This means that fitting the binding energies and the nd scattering length with either V_E^τ or V_E^I alone leads to an ambiguity in the expectation value of the potential.

By expanding the cutoff function

$$F_\Lambda(q^2) = e^{-q^4/\Lambda^4} \sim 1 - \frac{q^4}{\Lambda^4} + O\left(\frac{q^8}{\Lambda^8}\right), \tag{32}$$

one finds

$$V_E^\tau(3:12) = V_0^E \tau_{12} \left[\delta(r_{13}) \delta(r_{23}) + O\left(\frac{q^4}{\Lambda^4}\right) \right],$$
$$V_E^I(3:12) = V_0^E \left[\delta(r_{13}) \delta(r_{23}) + O\left(\frac{q^4}{\Lambda^4}\right) \right], \tag{33}$$

implying that in PNM

$$\langle V_E^{I,\tau}(3:12) \rangle_{\text{PNM}} = O\left(\frac{q^4}{\Lambda^4}\right). \tag{34}$$

From the above equation it becomes apparent that the expectation value of the three-nucleon potential, as well as its sign ambiguity, is nothing but a cutoff effect. Hence, it should

be regarded as a theoretical uncertainty. Note that, because $\Lambda_\chi \simeq \Lambda$, $\langle V_E \rangle_{\text{PNM}}$ is of the same order of the next term in chiral expansion.

To clarify this issue, let us consider a simple system: a Fermi gas of neutrons, in which correlations among particles are not present. The expectation value of the contact interaction reads

$$\frac{\langle V_E^{I,\tau} \rangle_{\text{PNM}}^{\text{FG}}}{A} = \frac{\rho^2}{2} V_0^E \int d^3r_{12} d^3r_{13} Z_0(r_{12}) Z_0(r_{13})$$
$$\times \left[1 - \frac{\ell(r_{12})^2}{2} - \frac{\ell(r_{13})^2}{2} - \frac{\ell(r_{23})^2}{2} \right.$$
$$\left. + \frac{\ell(r_{12})\ell(r_{13})\ell(r_{23})}{2} \right], \tag{35}$$

where A is the number of neutrons. The factor $1/2$ includes the $1/3!$ arising from the unrestricted sum over particle indices 123, multiplied by a factor 3 from the cyclic permutations of the potential, all giving the same contribution. The Slater function $\ell(r_{ij})$, for a system of fermions with degeneracy d is given by

$$\ell(r_{ij}) = \frac{d}{N} \sum_{|\mathbf{k}|<k_F} e^{-i\mathbf{k}_n\cdot\mathbf{r}_i} e^{i\mathbf{k}_n\cdot\mathbf{r}_j}$$
$$= 3\left[\frac{\sin(k_F r_{ij}) - k_F r_{ij} \cos(k_F r_{ij})}{(k_F r_{ij})^3} \right], \tag{36}$$

where $k_F = (\frac{6\pi^2 \rho}{d})^{1/3}$ is the Fermi momentum. It can be easily seen that, if $V_E^{I,\tau}(1:23) \propto \delta(r_{12})\delta(r_{13})$, then

$$\frac{\langle V_E^I \rangle_{\text{PNM}}^{\text{FG}}}{A} = 0. \tag{37}$$

Consider now a Fermi gas with equal numbers of protons and neutrons, where

$$\frac{\langle V_E^\tau \rangle_{\text{SNM}}^{\text{FG}}}{A} = \frac{\rho^2}{2} V_0^E \int d^3r_{12} d^3r_{13} Z_0(r_{12}) Z_0(r_{13})$$
$$\times \left[-\frac{3}{4}\ell(r_{23})^2 + \frac{3}{8}\ell(r_{12})\ell(r_{13})\ell(r_{23}) \right] \tag{38}$$

and

$$\frac{\langle V_E^I \rangle_{\text{SNM}}^{\text{FG}}}{A} = \frac{\rho^2}{2} V_0^E \int d^3r_{12} d^3r_{13} Z_0(r_{12}) Z_0(r_{13})$$
$$\times \left[1 - \frac{\ell(r_{12})^2}{4} - \frac{\ell(r_{13})^2}{4} - \frac{\ell(r_{23})^2}{4} \right.$$
$$\left. + \frac{\ell(r_{12})\ell(r_{13})\ell(r_{23})}{8} \right]. \tag{39}$$

In the limit of infinite cutoff the above equations imply

$$\frac{\langle V_E^{\tau_{12}} \rangle_{\text{SNM}}^{\text{FG}}}{A} = -\frac{3}{16} \rho^2 V_0^E,$$
$$\frac{\langle V_E^I \rangle_{\text{SNM}}^{\text{FG}}}{A} = \frac{3}{16} \rho^2 V_0^E. \tag{40}$$

As expected from Eq. (29), the two contributions have opposite signs.

TABLE III. Cutoff dependence of the expectation values of the three body contact term of the NNLOL potential in noninteracting PNM.

Λ (MeV)	$\langle V_E^{I,\tau_{12}} \rangle_{\text{PNM}}^{\text{FG}}/A$ (MeV)
300	9.15
400	5.95
500	3.60
600	2.15
700	1.30
800	0.81
∞	0

We have computed the expectation values of Eqs. (35), (38), and (39) for different values of the cutoff Λ and density $\rho = 0.16$ fm^{-3}. The results listed in Table III show that for PNM the larger the cutoff the smaller is the expectation value of the three-nucleon contact term. Note that for $\Lambda = 500$ MeV, the expectation value is still sizably different from the asymptotic limit.

As far as SNM is concerned (see Table IV), as the cutoff increases the possible choices of the three-nucleon contact term tend to the asymptotic values of Eq. (40). As in the case of PNM, the results corresponding to $\Lambda = 500$ MeV are significantly different from the asymptotic values.
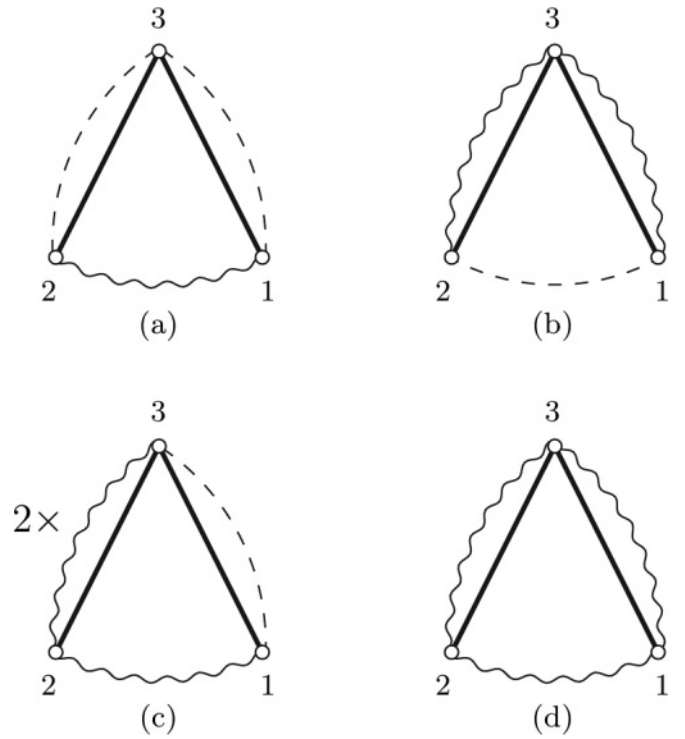
We emphasize that the parameter c_E has not been included in this analysis, even though it is itself cutoff dependent. Unfortunately, the authors of Ref. [19] kept Λ fixed to 500 MeV. Had this not been the case, their fit to the experimental data would have resulted in a set of different constants c_E, corresponding to different values of Λ. It would have been interesting to extrapolate the expectation value of V_E to the limit of infinite Λ, where the cutoff effects associated with the regularization procedure are expected to vanish.

B. FHNC/SOC calculations

The diagrams involved in the FHNC/SOC calculation of the expectation values of the $V^{2\pi}$ and V^R terms of the UIX potential are depicted in Figs. 3 and 4, respectively. The thick lines represent the potential, while dashed and wavy lines correspond to generalized scalar and operatorial correlations, denoted by Z^c and Z^p in Ref. [21], respectively. Double wavy lines represent single operator rings (SORs), while vertex corrections, although included in the calculations, are not

TABLE IV. Same as in Table III, but for SNM.

Λ (MeV)	$\langle V_E^{\tau_{12}} \rangle_{\text{SNM}}^{\text{FG}}/A$ (MeV)	$\langle V_E^{I} \rangle_{\text{SNM}}^{\text{FG}}/A$ (MeV)
300	−2.61	10.21
400	−3.61	8.15
500	−4.37	6.93
600	−4.87	6.30
700	−5.15	5.98
800	−5.30	5.81
∞	−5.55	5.55

FIG. 3. Cluster diagrams contributing to the expectation value of $V^{2\pi}$.

shown. The definitions of all these quantities can be found in Refs. [39,40].

Note that, because of the symmetry properties of the wave function, we can restrict our analysis to the permutation (3 : 12). Taking into account the other permutations results in the appearance of a multiplicative factor.

The computation of diagrams 3(a), 3(b), and 3(c) and all diagrams of Fig. 4 is outlined in Ref. [21], while the contribution of digram 3(d), involving three noncentral correlations was first taken into account by the authors of Ref. [23].

Using the relations for the constants and the radial functions given in Eqs. (23) and (24), the computation of the diagrams of Fig. 3 with the V_3 and V_4 terms of both the TM$'$ and NNLOL potentials is the same as that of $\hat{V}^{2\pi}$ reported in Ref. [21].

Thanks to the identity

$$(\boldsymbol{\sigma}_1 \cdot \hat{r}_{13})(\boldsymbol{\sigma}_2 \cdot \hat{r}_{23})(\hat{r}_{13} \cdot \hat{r}_{23}) = \tfrac{1}{18}\{\sigma_{13} + S_{13}, \sigma_{23} + S_{23}\},$$ (41)

the term V_1 of Eq. (7), appearing in both the TM$'$ and the NNLOL potentials, can be written in the form

$$V_1(3:12) = \frac{W_0}{36}\{\tau_{13}, \tau_{23}\}\{\sigma_{13} + S_{13}, \sigma_{23} + S_{23}\}$$
$$\times \frac{r_{13}r_{23}}{(\hat{r}_{13} \cdot \hat{r}_{23})} y(r_{13})y(r_{23}).$$ (42)

Aside from the radial function, V_1 is completely equivalent to V_3, the anticommutator term of the UIX potential. Therefore, we were allowed to use again the results of Ref. [21].
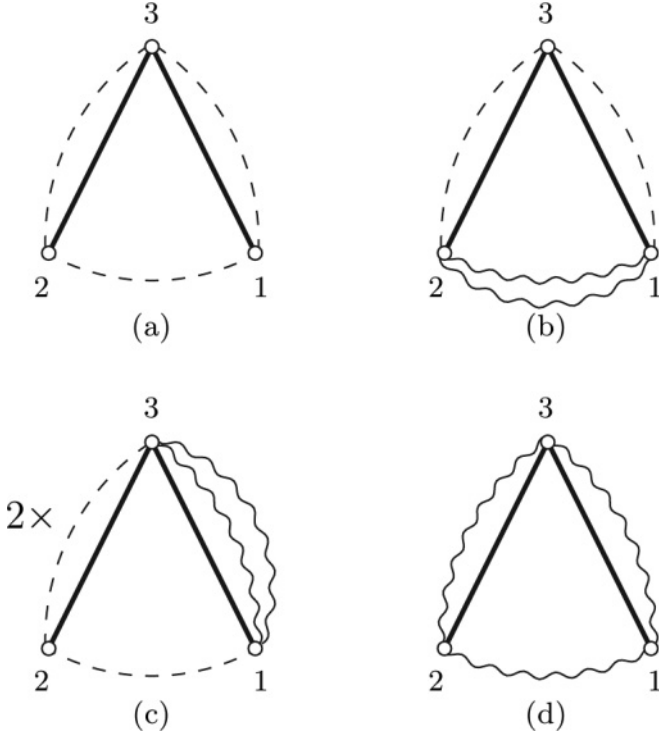
FIG. 4. Same as in Fig. 3, but for V^R.

Furthermore, exploiting the identities

$$(\boldsymbol{\sigma}_1 \cdot \vec{r}_{23})(\boldsymbol{\sigma}_2 \cdot \vec{r}_{23}) = \frac{r_{23}^2}{6}\{S_{23} + \sigma_{23}, \sigma_{13}\},$$
$$(\boldsymbol{\sigma}_2 \cdot \vec{r}_{13})(\boldsymbol{\sigma}_1 \cdot \vec{r}_{13}) = \frac{r_{13}^2}{6}\{\sigma_{23}, S_{13} + \sigma_{13}\},$$

(43)

we can rewrite the V_D term in a form that has again the same spin-isospin structure as the anticommutator contribution of the UIX potential,

$$
\begin{aligned}
V_D(3:12) = \frac{W_0^D}{4}\{\tau_{13}, \tau_{23}\}\big[\{\sigma_{13}, \sigma_{23}\}V_D^{YY}(r_{13}, r_{23}) \\
+ \{S_{13}, \sigma_{23}\}V_D^{TY}(r_{13}, r_{23}) \\
+ \{\sigma_{13}, S_{23}\}V_D^{YT}(r_{13}, r_{23})\big],
\end{aligned}
$$

(44)

where

$$
\begin{aligned}
V_D^{YY}(r_{13}, r_{23}) &= Y(r_{13})z_0(r_{23}) + z_0(r_{13})Y(r_{23}), \\
V_D^{YT}(r_{13}, r_{23}) &= z_0(r_{13})T(r_{23}), \\
V_D^{TY}(r_{13}, r_{23}) &= T(r_{13})z_0(r_{23}).
\end{aligned}
$$

(45)

In conclusion, including V_D amounts to properly adding the above radial functions to those already appearing in V_3.

The V_E term of TM$'$ is completely equivalent to V_R [see Eq. (26)]. This allowed us to use the results of Ref. [21] for the diagrams of Fig. 4. The same holds true for the chiral contact term V_E in PNM, as $\langle\tau_{ij}\rangle_{\text{PNM}} = 1$, while in SNM the calculation of V_E requires the evaluation of the diagrams of Fig. 3.

The expression of diagram 3(a) is

$$
\begin{aligned}
(3a) = \frac{c_E}{2}\rho^2 \sum_{ex}\sum_p \int d^3r_{12}d^3r_{13} Z_{xy,13}^c Z_{x'y',23}^c \\
\times Z_{x''y'',12}^p \mathrm{C}\big[V_E(3:12)O_{12}^p\big].
\end{aligned}
$$

(46)

As pointed out in Ref. [21], integrating and tracing over the radial and spin-isospin variables of particle 3 leads to the appearance of an effective density-dependent interaction

$$
\begin{aligned}
\sum_p V_{E,yy',12}^p(\rho)O_{12}^p = \rho\sum_{ex}\int d^3r_{13} Z_{xy,13}^c Z_{x'y',23}^c \\
\times \mathrm{C}_3[V_E(3:12)],
\end{aligned}
$$

(47)

such that

$$
(3a) = \frac{c_E}{2}\rho\sum_{ex}\sum_p\int d^3r_{12} A^p Z_{x''y'',12}^p V_{E,yy',12}^p(\rho).
$$

(48)

The subscripts xy label exchange patterns at the ends of the generalized correlation lines. In particular, dd stands for direct-direct, de for direct-exchange, ee for exchange-exchange, and cc for incomplete circular exchange. The matrix A_p is defined through [40]

$$
\mathrm{C}\big(O_{ij}^p O_{ij}^q\big) = \delta^{pq}A^p,
$$

(49)

implying $A^p = 1, 3, 3, 9, 6, 18$ for $p = 1, \dots, 6$.

It turns out that the only nonvanishing term of the density dependent potential is

$$
V_{E\,yy',12}^\tau(\rho) = W_0^E \rho\sum_{ex}\int d^3r_{13} Z_{xy,13}^c Z_{x'y',23}^c z_0(r_{13})z_0(r_{23}).
$$

(50)

The contribution of diagram 3(b) is given by

$$
\begin{aligned}
(3b) = \frac{c_E}{2}\rho^2\sum_{ex}\sum_{p,p'}\int d^3r_{12}d^3r_{13} Z_{xy,13}^p Z_{x'y',23}^{p'} \\
\times Z_{x''y'',12}^c \mathrm{C}\left(V_E(3:12)\frac{1}{2}\{O_{13}^p, O_{23}^{p'}\}\right).
\end{aligned}
$$

(51)

From the above expression, it clearly follows that only τ-type generalized correlation lines contribute. Hence,

$$
\begin{aligned}
(3b) = \frac{3}{2}c_E W_0^E \rho^2\sum_{ex}\int d^3r_{12}d^3r_{13} Z_{xy,13}^\tau Z_{x'y',23}^\tau \\
\times Z_{x''y'',12}^c z_0(r_{13})z_0(r_{23}).
\end{aligned}
$$

(52)

Diagram 3(c) does not contribute to V_E, while for diagram 3(d), with three generalized operatorial correlation, we find

$$
\begin{aligned}
(3d) = \frac{c_E}{2}\rho^2\sum_{ex}\sum_{p,p',p''}\int d^3r_{12}d^3r_{13} Z_{xy,12}^p Z_{x'y',13}^{p'} \\
\times Z_{x''y'',23}^{p''}\mathrm{C}\bigg[\frac{V_E(3:12)}{3!}\big(O_{12}^p\{O_{13}^{p'}, O_{23}^{p''}\} \\
+ O_{13}^{p'}\{O_{12}^p, O_{23}^{p''}\} + O_{23}^{p''}\{O_{12}^p, O_{13}^{p'}\}\big)\bigg].
\end{aligned}
$$

(53)

The calculation of the spin-isospin traces yields

$$
\begin{aligned}
(3d) = \frac{c_E}{2} W_0^E \rho^2 \int d^3 r_{12} d^3 r_{13} \big(&-2 Z_{12}^\tau Z_{13}^\tau Z_{23}^\tau + 9 Z_{12}^{\sigma\tau} Z_{13}^\sigma Z_{23}^\sigma \\
&+ 9 Z_{12}^\sigma Z_{13}^{\sigma\tau} Z_{23}^{\sigma\tau} - 6 Z_{12}^\sigma Z_{13}^{\sigma\tau} Z_{23}^{\sigma\tau} + 18 \xi_{231}^{\sigma t t} Z_{12}^t Z_{13}^{t\tau} Z_{23}^{\sigma\tau} \\
&- 12 \xi_{231}^{\sigma t t} Z_{12}^{t\tau} Z_{13}^{t\tau} Z_{23}^{\sigma\tau} + 18 \xi_{231}^{t\sigma t} Z_{12}^t Z_{13}^\sigma Z_{23}^{t\tau} \\
&+ 18 \xi_{231}^{t\sigma t} Z_{12}^{t\tau} Z_{13}^\sigma Z_{23}^t - 12 \xi_{231}^{t\sigma t} Z_{12}^{t\tau} Z_{13}^\sigma Z_{23}^{t\tau} \\
&+ 9 \xi_{231}^{t t\sigma} Z_{12}^\sigma Z_{13}^{t\tau} Z_{23}^{t\tau} + 9 \xi_{231}^{t t\sigma} Z_{12}^{\sigma\tau} Z_{13}^t Z_{23}^t \\
&- 6 \xi_{231}^{t t\sigma} Z_{12}^{\sigma\tau} Z_{13}^{t\tau} Z_{23}^{t\tau} - 12 \xi_{231}^{t t t} Z_{12}^{t\tau} Z_{13}^{t\tau} Z_{23}^{t\tau} \\
&+ 18 \xi_{231}^{t t t} Z_{12}^t Z_{13}^{t\tau} Z_{23}^{t\tau} + 18 \xi_{231}^{t t t} Z_{12}^{t\tau} Z_{13}^t Z_{23}^t \\
&+ 18 \xi_{231}^{\sigma t t} Z_{12}^{t\tau} Z_{13}^t Z_{23}^\sigma \big) z_0(r_{13}) z_0(r_{23}).
\end{aligned} \tag{54}
$$

The matrices ξ_{231}^{pqr}, depending on the angles formed by the vectors $\mathbf{r}_1$, $\mathbf{r}_2$, and $\mathbf{r}_3$, are defined in Ref. [40]. Following Ref. [23] we have considered only the direct term of the generalized operatorial correlations. As a consequence, in the previous equation $Z_{ij}^p = Z_{dd,ij}^p$.

To find the optimal values of the variational parameters, we have employed a procedure similar to simulated annealing, the details of which are explained in Ref. [26].

The authors of Ref. [26] constrained the difference between the Pandharipande-Bethe (PB) and the Jackson-Feenberg (JF) kinetic energies to be less than 10% of the Fermi energy T_F and required the sum rule involving the scalar two-body distribution function, $g^c(r_{12})$, to be fulfilled with a precision of 3%. In variational calculations of SNM we have imposed the further condition, first considered in Ref. [23], that the sum rule of the isospin component of the two-body distribution function,

$$
\rho \int d\vec{r}_{12} g^\tau(r_{12}) = -3, \tag{55}
$$

be also satisfied to the same accuracy.

Using also the sum rules for the spin and spin-isospin two-body distribution functions leads to a sizable increase of the variational energies, which turn out to be much higher than those obtained releasing the additional constraints, as well as the AFDMC results. The same pattern is observed in the results of variational calculations not including TNFs. For this reason, we have enforced the fulfillment of the sum rules for $g^c(r_{12})$ and $g^\tau(r_{12})$ only.

For potentials other than UIX, it turns out that the variational energies of PNM resulting from our optimization procedure are lower than the AFDMC values at $\rho > \rho_0$. By carefully analyzing the contributions of the cluster expansion diagrams, we realized that the value of diagram 3(a) was unnaturally large. In particular, we have found that a small change in the variational parameters leads to a huge variation of the value of the diagram. Moreover, the minimum of the energy in parameter space was reached in a region where the kinetic energy difference was very close to the allowed limit.

To cure this pathology, we have constrained the PB-JF kinetic energy difference to be less than 1 MeV, regardless of density. The variational energies obtained imposing this new constraint are always larger than the corresponding AFDMC values and the value of diagram 3(a) is brought under control. For the sake of consistency, the same constraint on the kinetic energies has been also applied to SNM. In addition, the variational energy minimum does not correspond to the maximum allowed violation of the constraints. As a consequence, it would be largely unaffected by a slight modification of the constraints.

C. AFDMC calculations

We have computed the EoS of PNM using the AFDMC approach [41] with the TM′ and NNLOL chiral potentials combined with the Argonne $v_8' NN$ interaction.

The agreement between Green's function Monte Carlo (GFMC) and AFDMC energies of neutron drops, obtained using the Argonne v_8' plus UIX hamiltonian, discussed in Ref. [42], supports the validity of PNM calculations carried out within AFDMC with the Argonne v_8' model. The highly accurate GFMC method has been used to study neutron matter properties in both the normal [43] and the superfluid [44] phases. However, for interactions involving the spin coupling $\boldsymbol{\sigma}_i \cdot \boldsymbol{\sigma}_j$, such as Argonne v_8', the computational cost of GFMC calculations grows exponentially with the number of neutrons. Hence, so far, GFMC simulations have only been carried out using periodic boxes with at most 14 neutrons.

An efficient procedure for performing AFDMC calculations with three-body potentials is described in Ref. [45]. Because V_3 is equivalent to the anticommutator term of the UIX model (while the commutator, V_4, is zero in PNM), and in PNM the V_E terms of both the TM′ and the NNLOL potentials do not show any formal difference with respect to the repulsive term of UIX, the inclusion of these terms reduces to a replacement of constants and radial functions. The authors of Ref. [45] also described how to handle the V_1 for the TM model, and no further difficulties arise in the case of the NNLOL potential.

As the V_D term has never been encompassed in AFDMC, it is worthwhile showing how the calculation of this term reduces to a matrix multiplication. The expectation value of V_D is given by

$$
\langle V_D \rangle = \sum_{i<j<k} [V_D(i:jk) + V_D(j:ik) + V_D(k:ij)], \tag{56}
$$

with $V_D(i:jk) = V_D(i:kj)$ (otherwise, all six permutations need to be summed). Thanks to this property one can write

$$
\langle V_D \rangle = \sum_{i<k,j} V_D(j:ik). \tag{57}
$$

It is possible to write $V_D(j:ik)$ of Eq. (44) in terms of Cartesian components operators

$$
\begin{aligned}
V_D(j:ik) = (&Y_{\alpha i;\beta j} Z_{\gamma j;\delta k} + Z_{\alpha i;\beta j} Y_{\gamma j;\delta k} + T_{\alpha i;\beta j} Z_{\gamma j;\delta k} \\
&+ Z_{\alpha i;\beta j} T_{\gamma j;\delta k}) \{ \sigma_i^\alpha \sigma_j^\beta, \sigma_j^\gamma \sigma_k^\delta \},
\end{aligned} \tag{58}
$$

where

$$
\begin{aligned}
Y_{\alpha i;\beta j} &= Y(r_{ij}) \delta^{\alpha\beta}, \\
Z_{\alpha i;\beta j} &= z_0(r_{ij}) \delta^{\alpha\beta}, \\
T_{\alpha i;\beta j} &= T(r_{ij}) \big(3 \hat{r}_{ij}^\alpha \hat{r}_{ij}^\beta - \delta^{\alpha\beta} \big).
\end{aligned} \tag{59}
$$

The anticommutation relation $\{\sigma_i^\alpha, \sigma_j^\beta\} = 2\delta^{\alpha\beta}$ makes the expectation value of V_D a sum of $3N \times 3N$ matrix multiplications

$$\langle V_D \rangle = 2 \sum_{i<k, j} (Y_{\alpha i; \beta j} Z_{\beta j; \delta k} + Z_{\alpha i; \beta j} Y_{\beta j; \delta k}$$
$$+ T_{\alpha i; \beta j} Z_{\beta j; \delta k} + Z_{\alpha i; \beta j} T_{\beta j; \delta k}) \sigma_i^\alpha \sigma_k^\delta$$
$$= 2 \sum_{i<k} (\{Y, Z\} + \{T, Z\})_{\alpha i; \delta k} \sigma_i^\alpha \sigma_k^\delta, \qquad (60)$$

analogous to those of Ref. [45]. To compute the expectation value of V_D the former expression has been added to the Cartesian matrices associated with the two-body potential.

Following Ref. [26], we simulated PNM with $A = 66$ neutrons in a periodic box, as described in Refs. [46,47], using the fixed-phase approximation. For 66 neutrons finite-size effects on the kinetic energy have been found to be small, as its value is very close to the thermodynamic limit. Moreover, as shown in Ref. [47], the energy per particle obtained with 66 neutrons imposing the periodic box condition (PBC) differs by no more than 2% from the asymptotic value calculated with twist-averaged boundary conditions (TABCs).

Finite-size effects are expected to be larger when the density is bigger, as the dimension of the box decreases. To check the validity of our calculations, at $\rho = 0.48$ fm^{-3} we have repeated the calculation with 114 neutrons. For all the potentials, the energies per particle obtained with 114 neutrons are higher than those obtained with 66 neutrons. The authors of Ref. [47] found a similar behavior for PNM at $\rho \leqslant 0.32$ fm^{-3} in the case of the v_8' plus UIX Hamiltonian and ascribed part of this difference to the Fermi gas energy, amounting to 72.63 MeV and at 74.15 MeV for 66 and 114 neutrons, respectively. However, the difference of the energy per particle obtained with 66 and 114 neutrons is always within 4 MeV. It is worth noting that once finite-size effects on the Fermi gas energy are accounted for, the residual finite-size effects do not exceed 4% of the energy per particle. Finally, as the free-gas value obtained with 66 neutrons turns out to be very close to the thermodynamic limit of 73.00 MeV, the finite size corrections for 66 neutrons tend to be small.

IV. NUCLEAR-MATTER EOS

A. TM′ potential

The results of Fig. 5, showing the density dependence of the energy per nucleon in PNM, indicate that, once the new constraint on the difference between PB and JF kinetic energies is imposed, the agreement between FHNC/SOC (solid line) and AFDMC (triangles) results is very good.

The most striking feature of the results displayed in Fig. 6 is that, despite the parameters of the three-body potentials being different, all SNM EoS obtained from the TM′ potential turn out to be very close to each other. This is probably attributable to the fact that these potentials are designed to reproduce not only the binding energies of ^{3}H and ^{4}He, but also the nd doublet scattering length $^2a_{nd}$.
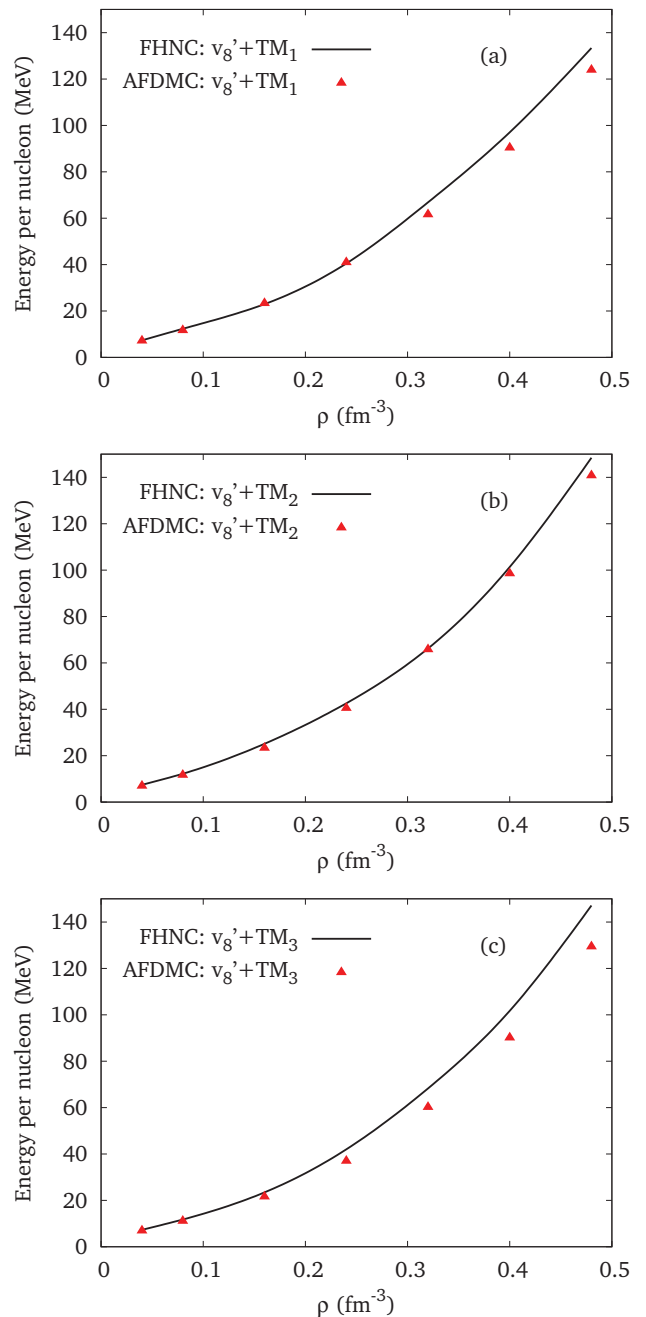

FIG. 5. (Color online) Equation of state of PNM obtained using the AFDMC (triangles) and FHNC/SOC (solid lines) approaches with the TM$_1'$ (a), TM$_2'$ (b), and TM$_3'$ (c) plus v_8' Hamiltonian.

It is remarkable that although the parameters of TM′ potentials were not adjusted to reproduce nuclear-matter properties, the EoS saturates at densities only slightly lower than $\rho_0 = 0.16$ fm^{-3}, and the compressibilities are in agreement with the experimental value $K \approx 240$ MeV. However, the binding energies are larger than the empirical value $E_0 = -16$ MeV and rather close to the one obtained from the UIX potential, ~ 10 MeV [26]. The numerical values of all these quantities are listed in Table V.
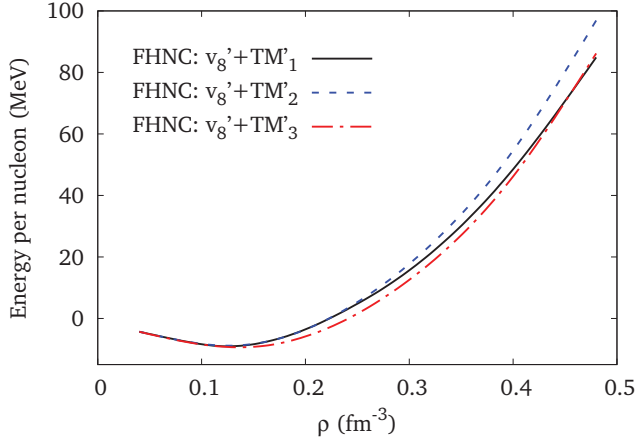
FIG. 6. (Color online) Equation of state of SNM resulting from FHNC/SOC variational calculations with the TM′ plus v_8' Hamiltonian.

TABLE V. Saturation density, binding energy per particle, and compressibility of SNM corresponding to the TM′ EoS displayed in Fig. 6.

	TM′$_1$	TM′$_2$	TM′$_3$
ρ_0 (fm^{-3})	0.12	0.13	0.14
E_0 (MeV)	-9.0	-8.8	-9.4
K (MeV)	266	243	249

The EoS of Fig. 7 are softer than those obtained from both the TM′ (compare to Fig. 5), and UIX (see, e.g., Fig. 12 of Ref. [26]) potentials. This is attributable to the ambiguity in the term V_E, discussed in Sec. III A.

In the NNLOL$_2$, NNLOL$_3$, and NNLOL$_4$ models the constant c_E is negative. Therefore, the contribution of V_E is attractive, making the EoS very soft. When V_E is repulsive (i.e., c_E is positive), as in the NNLOL$_1$ potential, its contribution is very small and the resulting EoS, while being stiffer than those corresponding to the other NNLOL potentials, remains very soft.

The recent astrophysical data of Ref. [20] suggest that the EoS of PNM be at least as stiff as the one obtained with a readjusted version of the effective density-dependent potential of Lagaris and Pandharipande in combination with the Argonne v_6' two-body interaction [48]. Therefore, the

B. NNLOL chiral potentials

The results displayed in Fig. 7 show that, as in the case of the TM′ potentials, the EoS of PNM computed within the AFDMC and FHNC/SOC schemes are very close to each other over the entire density range.
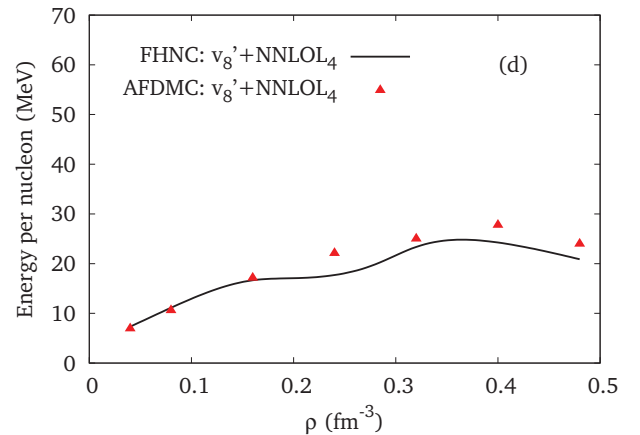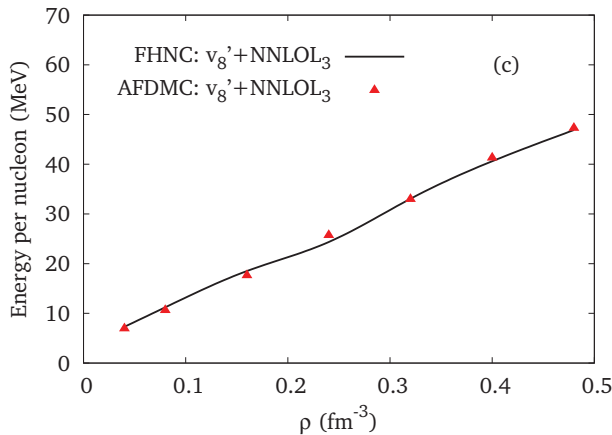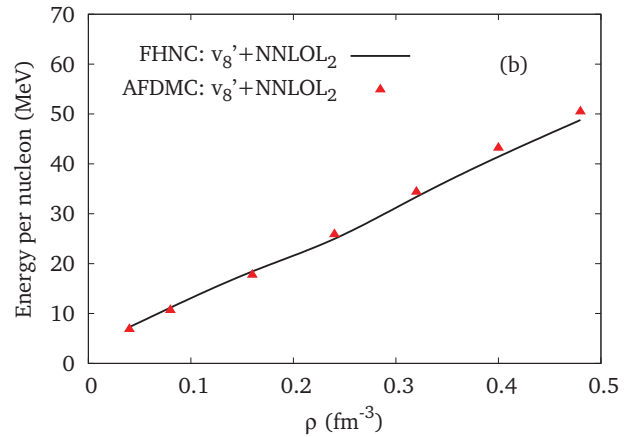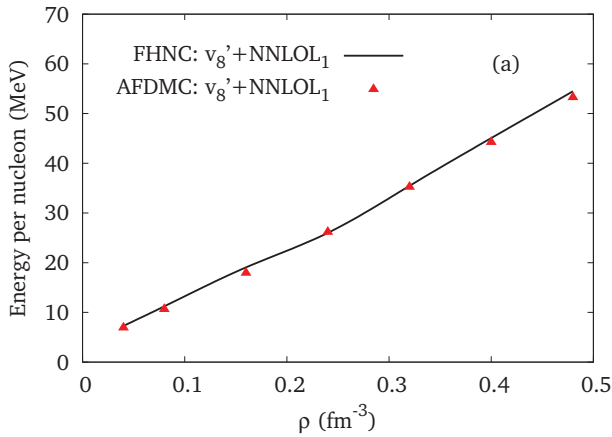

FIG. 7. (Color online) Same as Fig. 5, but for NNLOL$_1$ (a), NNLOL$_2$ (b), NNLOL$_3$ (c), and NNLOL$_4$ (d) plus v_8' Hamiltonian.
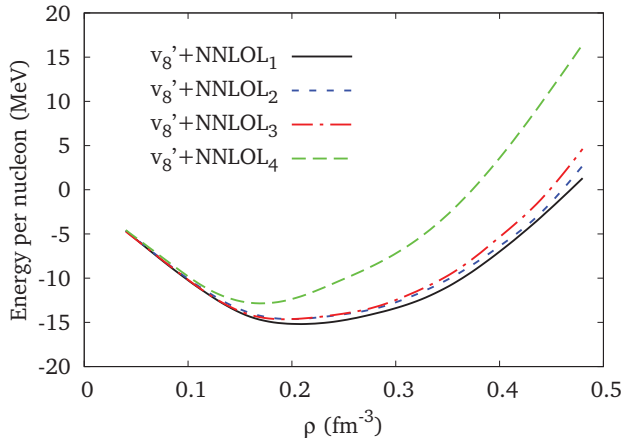
FIG. 8. (Color online) Same as Fig. 6, but for NNLOL plus v_8' Hamiltonian.

EoS resulting from chiral NNLOL potentials are not likely to describe a neutron star of mass around $2M_\odot$.

The SNM EoS corresponding to the NNLOL potentials are displayed in Fig. 8. The fact that the NNLOL$_4$ potential provides the stiffest EoS, while in PNM provided the softest, is not surprising. As discussed in Sec. III A, when the contact term is attractive in PNM, it is repulsive in SNM, and vice versa. A large cancellation between the repulsive core of the Argonne v_8' and the strong attractive contact term contribution of the NNLOL$_4$ potential is observed. This could influence the variational results, which for this particular three-body force could be less accurate than for the other interactions. As the corresponding AFDMC results do not show a similar behavior, giving a simple physical interpretation to the inflection point at $\rho \simeq 0.24$ fm^{-3} resulting from the FHNC/SOC calculations turns out to be difficult.

The results listed in Table VI show that none of the chiral NNLOL potentials fulfills the empirical constraints on the SNM EoS. All potentials overestimate the saturation density, while the compressibility is compatible with the empirical value only for the NNLOL$_2$ and NNLOL$_3$ models. As for the binding energies, they are closer to the experimental value than those obtained using both the UIX and TM$'$ potentials.

As a final remark, it has to be noticed that using the scalar repulsive term V_E^I instead of V_E^τ provides more repulsion, resulting in a stiffer EoS. As stressed in Sec. III A, this issue needs to be addressed, taking into account all terms that become equivalent in the limit of infinite cutoff only. Moreover, because the discrepancies among these terms are of the same order as the NNNLO term of the chiral expansion, other contact terms have to be included [49].

TABLE VI. Saturation density, the binding energy per particle, and the compressibility related to the NNLOL EoS displayed in Fig. 8.

	NNLOL$_1$	NNLOL$_2$	NNLOL$_3$	NNLOL$_4$
ρ_0 (fm^{-3})	0.21	0.20	0.19	0.17
E_0 (MeV)	-15.2	-14.6	-14.6	-12.9
K (MeV)	198	252	220	310

V. CONCLUSIONS

A new generation of chiral inspired three-nucleon potentials in coordinate space, suitable for carrying out nuclear-matter calculations, is now available. We have carried out a comparative analysis of the EoS of PNM and SNM obtained using the different parametrizations of the NNLOL potential, as well as the improved versions of the TM model discussed in Ref. [19].

The calculation of the SNM EoS has been been performed within the variational FHNC/SOC approach. In the case of PNM we have also used the AFDMC computational scheme, the results of which turn out to be in close agreement with the variational FHNC/SOC estimates.

Our analysis shows that the transformation from momentum to coordinate space brings about a cutoff dependence, leading to sizable effects in nuclear matter. As discussed in Sec. III A, the contribution of the contact term, which in PNM would vanish in the $\Lambda \to \infty$ limit, cannot be fully determined fitting the low-energy observables. Moreover, the *NNN* contact terms of the NNLOL$_2$ and NNLOL$_3$ models turn out to be attractive in PNM, leading to a strong softening of the EoS.

An illustrative example of the uncertainty associated with the local form of the *NNN* contact term is provided by the results of Fig. 8 and Table VI. The NNLOL$_4$ model largely overestimates the empirical value of the compressibility modulus of SNM, thus yielding a stiff EoS. However, as pointed out in Sec. IV B, it predicts a soft EoS of PNM. The impact of this is ambiguity is large, because compressibility is a most important property of the EoS. The recent discovery of a $\sim 2M_\odot$ neutron star appears, in fact, to rule out dynamical models yielding a soft EoS of β-stable matter.

None of the considered three-nucleon potential models simultaneously explains the empirical equilibrium density and binding energy of SNM. However, among the different parametrization that we have analyzed, the NNLOL$_4$ and TM$'_3$ provide reasonable values of ρ_0. It has to be emphasized that this is a remarkable result, as, unlike the UIX model, these potentials do not involve any parameter adjusted to reproduce ρ_0.

To resolve the inconsistencies involved in the contact term, one should include all contributions to this term arising from the chiral expansion at NNLO. Moreover, as pointed out by the authors of Ref. [49], owing to the choice of the regulator function [see Eq. (6)], a fully consistent treatment should also take into account NNNLO contact contributions.

As a final remark, it must be mentioned that the TM$'$ and NNLOL potentials discussed in this paper can be used to obtain two-body density-dependent effective interaction within the formalism developed in Ref. [26]. At present, this is the only approach allowing for the inclusion of three-nucleon potentials involving a term of the form of V_4 of Eq. (7) in AFDMC calculations of SNM.

[1] M. Lacombe, B. Loiseau, J. M. Richard, R. Vinh Mau, J. Cônté, P. Pirès, and R. de Tourreil, Phys. Rev. C **21**, 861 (1980).

[2] V. G. J. Stoks, R. A. M. Klomp, C. P. F. Terheggen, and J. J. de Swart, Phys. Rev. C **49**, 2950 (1994).

[3] R. B. Wiringa, V. G. J. Stoks, and R. Schiavilla, Phys. Rev. C **51**, 38 (1995).

[4] R. Machleidt, Phys. Rev. C **63**, 024001 (2001).

[5] D. R. Entem and R. Machleidt, Phys. Rev. C **68**, 041001(R) (2003).

[6] E. Epelbaum, W. Glöckle, Ulf-G. Meißner, Nucl. Phys. A **747**, 362 (2005).

[7] V. G. J. Stoks, R. A. M. Klomp, M. C. M. Rentmeester, and J. J. de Swart, Phys. Rev. C **48**, 792 (1993).

[8] B. Gabioud, J.-C. Alder, C. Joseph, J.-F. Loude, N. Morel, A. Perrenoud, J.-P. Perroud, M. T. Tran, E. Winkelmann, W. Dahme, H. Panke, D. Renker, Č. Zupančič, G. Strassner and P. Truöl, Phys. Rev. Lett. **42**, 1508 (1979).

[9] C. van der Leun and C. Alderlisten, Nucl. Phys. A **380**, 261 (1982).

[10] T. E. O. Ericson and M. Rosa-Clot, Nucl. Phys. A **405**, 497 (1983).

[11] N. L. Rodning and L. D. Knutson, Phys. Rev. C **41**, 898 (1990).

[12] G. G. Simon, Ch. Schmitt, and V. H. Walther, Nucl. Phys. A **364**, 285 (1981).

[13] D. M. Bishop and L. M. Cheung, Phys. Rev. A **20**, 381 (1979).

[14] K. Schoen, D. L. Jacobson, M. Arif, P. R. Huffman, T. C. Black, W. M. Snow, S. K. Lamoreaux, H. Kaiser, and S. A. Werner, Phys. Rev. C **67**, 044005 (2003).

[15] S. Shimizu, K. Sagara, H. Nakamura, K. Maeda, T. Miwa, N. Nishimori, S. Ueno, T. Nakashima, and S. Morinobu, Phys. Rev. C **52**, 1193 (1995).

[16] E. Epelbaum, A. Nogga, W. Glöckle, H. Kamada, Ulf-G. Meißner, and H. Witala, Phys. Rev. C **66**, 064001 (2002).

[17] V. Bernard, E. Epelbaum, H. Krebs, Ulf-G. Meißner, Phys. Rev. C **77**, 064004 (2008).

[18] P. Navratil, Few Body Syst. **41**, 117 (2007).

[19] A. Kievsky, M. Viviani, L. Girlanda, and L. E. Marcucci, Phys. Rev. C **81**, 044003 (2010).

[20] P. B. Demorest, T. Pennucci, S. M. Ransom, M. S. E. Roberts, and J. W. T. Hessels, Nature (London) **467**, 1081 (2010).

[21] J. Carlson, V. R. Pandharipande, and R. B. Wiringa, Nucl. Phys. A **401**, 59 (1983).

[22] S. A. Coon and W. Glöckle, Phys. Rev. C **23**, 1790 (1981)

[23] R. B. Wiringa, V. Fiks, and A. Fabrocini, Phys. Rev. C **38**, 1010 (1988).

[24] A. Akmal, V. R. Pandharipande, and D. G. Ravenhall, Phys. Rev. C **58**, 1804 (1998).

[25] B. S. Pudliner, V. R. Pandharipande, J. Carlson, and R. B. Wiringa, Phys. Rev. Lett. **74**, 4396 (1995).

[26] A. Lovato, O. Benhar, S. Fantoni, A. Yu. Illarionov, and K. E. Schmidt, Phys. Rev. C **83**, 054003 (2011).

[27] S. Gandolfi, F. Pederiva, S. Fantoni, and K. E. Schmidt, Phys. Rev. Lett. **98**, 102503 (2007).

[28] S. K. Bogner, A. Schwenk, R. J. Furnstahl, and A. Nogga, Nucl. Phys. A **763**, 59 (2005).

[29] K. Hebeler, S. K. Bogner, R. J. Furnstahl, A. Nogga, and A. Schwenk, Phys. Rev. C **83**, 031301 (2011).

[30] K. Hebeler and A. Schwenk, Phys. Rev. C **82**, 014314 (2010).

[31] S. Weinberg, Phys. Lett. B **251**, 288 (1990).

[32] S. Weinberg, Nucl. Phys. B **363**, 3 (1991)

[33] N. Fettes, U.-G. Meißner, S. Steiniger, Nucl. Phys. A **640**, 199 (1998).

[34] P. Büttiker and U.-G. Meißner, Nucl. Phys. A **668**, 97 (2000).

[35] V. Bernard, E. Epelbaum, H. Krebs, and Ulf-G. Meißner, Phys. Rev. C **84**, 054001 (2011).

[36] J. L. Friar, D. Hüber, and U. van Kolck, Phys. Rev. C **59**, 53 (1999).

[37] S. A. Coon and H. K. Ha, Few Body Syst **30**, 131 (2001).

[38] J. Fujita and H. Miyazawa, Prog. Theor. Phys. **17**, 360 (1957).

[39] R. B. Wiringa and V. R. Pandharipande, Nucl. Phys. A **299**, 1 (1978).

[40] V. R. Pandharipande and R. B. Wiringa, Rev. Mod. Phys. **51**, 821 (1979).

[41] K. E. Schmidt and S. Fantoni, Phys. Lett. B **446**, 99 (1999).

[42] S. Gandolfi, J. Carlson, and S. C. Pieper, Phys. Rev. Lett. **106**, 012501 (2011).

[43] J. Carlson, J. Morales Jr., V. R. Pandharipande, and D. G. Ravenhall, Phys. Rev. C **68**, 025802 (2003).

[44] A. Gezerlis and J. Carlson, Phys. Rev. C **81**, 025803 (2010).

[45] F. Pederiva, A. Sarsa, K. E. Schmidt, and S. Fantoni, Nucl. Phys. A **742**, 255 (2004).

[46] S. Fantoni, S. Gandolfi, A. Yu. Illarionov, K. E. Schmidt, and F. Pederiva, AIP Conf. Proc. **1056**, 233 (2008).

[47] S. Gandolfi, A. Yu. Illarionov, K. E. Schmidt, F. Pederiva, and S. Fantoni, Phys. Rev. C **79**, 054005 (2009).

[48] S. Gandolfi, A. Yu. Illarionov, S. Fantoni, J. C. Miller, F. Pederiva, and K. E. Schmidt, Mon. Not. R. Astron. Soc. **404**, L35 (2010).

[49] L. Girlanda, A. Kievsky, and M. Viviani, Phys. Rev. C **84**, 014001 (2011).